

Critical fluctuations of elastic moduli in jammed solids

Kumpei Shiraishi¹ and Hideyuki Mizuno²

¹*SANKEN, University of Osaka, 8-1 Mihogaoka, Ibaraki, Osaka 567-0047, Japan*

²*Graduate School of Arts and Sciences, University of Tokyo, 3-8-1 Komaba, Meguro, Tokyo 153-8902, Japan*

(Dated: February 10, 2026)

We investigate sample-to-sample fluctuations of the shear modulus in ensembles of particle packings near the jamming transition. Unlike the average modulus, which exhibits distinct scaling behaviours depending on the interparticle potential, the fluctuations obey a critical exponent that is independent of the potential. Furthermore, this scaling behaviour has been confirmed in two-dimensional packings, indicating that it holds regardless of spatial dimension. Using this scaling law, we discuss the relationship predicted by heterogeneous-elasticity theory between elastic-modulus fluctuations and the Rayleigh scattering of sound waves across different pressures. Our numerical results provide a useful foundation for developing a unified theoretical description of the jamming critical phenomenon.

I. INTRODUCTION

When particles are compressed, the system jams and acquires rigidity at a certain packing fraction. The phenomenon, called the jamming transition, is ubiquitous in diverse materials such as foams, colloidal suspensions, pastes, and granular materials, and forms a basis for understanding properties of disordered systems, spanning from structural glasses to biological systems [1, 2]. Over the past 30 years, various studies, including theoretical [3, 4], numerical [5, 6] and experimental [7, 8] approaches, have characterised basic properties of this phenomenon. The most central observation is made in critical phenomena; various physical quantities exhibit power-law scaling near the transition [5, 6]. This critical behaviour manifests in elastic moduli [6, 9], vibrations [10, 11], transport properties [12–14], and rheology [15]. Furthermore, at the transition point, the number of contacts exactly matches the number of degrees of freedom in the system, a state known as isostaticity [6]. It is now well established that the jamming scaling law is controlled by the contact number excess to the isostatic value [3, 4].

One of the central challenges in statistical physics is the understanding of phase transitions and critical phenomena [16–19]. In this context, theoretical tools such as mean-field theory and, more importantly, the renormalization group have been developed, and it has become clear that fluctuations play a crucial role in critical behaviour. In particular, as a system approaches a critical point, both the fluctuations and the associated correlation length scales diverge, leading to various anomalies at the critical point. In the field of jamming transition, some works have followed this line of research, including scaling collapse and finite-size scaling [9, 20, 21], diverging length scales [3, 10, 22, 23], and Widom scaling hypothesis [24]. Thus, understanding how fluctuations in physical quantities behave near the jamming critical point remains an important issue. Despite its relevance, the study of fluctuations in jamming systems is still limited, and further development is anticipated [25–28].

Beyond their relevance in statistical physics, fluctuations in elastic moduli play an essential role in the theoretical description of the anomalous properties of amorphous solids. Among the various theoretical frameworks [29–34], the heterogeneous-elasticity theory (HET) [35–39] is one of the most well-established approaches for describing the anomalous behaviour of amorphous materials such as jammed solids. HET postulates that the local shear modulus exhibits spatial fluctuations throughout the system, and extensive numerical studies have indeed confirmed the existence of such elastic heterogeneity in amorphous systems [40–42]. Within this theoretical framework, the so-called disorder parameter γ , which quantifies the variance of local shear moduli, acts as a key control parameter [36]. In the standard formulation of HET, the distribution of local shear moduli is assumed to be Gaussian, and its mean value and standard deviation serve as inputs for computing macroscopic observables. This formulation successfully accounts for a variety of universal features of amorphous solids. For example, the low-frequency vibrational modes in excess over the Debye prediction (the boson peak) can be captured within HET, with both their characteristic frequency and intensity expressed as functions of γ . Likewise, the theory predicts a Rayleigh-type frequency dependence of the acoustic attenuation, $\Gamma \sim \Omega^{d+1}$ (Γ is the attenuation coefficient and Ω is the propagation frequency), which is also observed in experiments on glasses [43, 44]. The prefactor of this relation, corresponding to the strength of Rayleigh scattering, is again determined by γ , linking vibrational and transport anomalies to the underlying elastic heterogeneity. These theoretical predictions, spanning both vibrational spectra [14, 45, 46] and acoustic attenuation [14, 47, 48], have been extensively tested through numerical simulations.

Another major theoretical framework developed to describe and predict the properties of amorphous solids is the effective medium theory (EMT), which is based on spring-network models [49]. While HET treats the spatial fluctuations of local shear moduli as the sole mesoscale input, EMT instead relies on microscopic parameters, namely the mean coordination number z and

the contact strain e , often referred to as the pre-stress. Despite this difference in the scale of description, EMT successfully reproduces the same key features of vibrational and scattering phenomena as HET, including the emergence of the boson peak and the Rayleigh-type acoustic attenuation. Given that both theories capture similar physical phenomena from different levels of description, it is natural to expect that they are connected via an appropriate coarse-graining procedure. However, the precise nature of this connection remains elusive. One major reason for this persistent gap is the limited numerical characterisation of fluctuations of elastic modulus. From this perspective, a detailed characterisation of local shear modulus fluctuations is of particular theoretical significance, particularly for bridging the gap between these two frameworks.

In this work, we characterise the sample-to-sample fluctuations of elastic moduli in ensembles of jammed packings by means of numerical simulation. These fluctuations are believed to encode information equivalent to the disorder parameter in HET [50, 51]. We focus on two prototypical models of jammed amorphous solids: harmonic spheres and Hertzian spheres. Our results reveal that, while the average elastic modulus exhibits a model-dependent scaling behaviour, its fluctuations diverge in a manner independent of the interaction potential. This critical scaling is also observed in two-dimensional packings. Finally, we discuss the theoretical implications of these findings, with particular emphasis on their relevance to the HET prediction on acoustic attenuation in amorphous solids.

II. METHODS

A. System description

We consider randomly jammed packings in a three-dimensional box with periodic boundary conditions. Particles interact with a finite-range purely repulsive potential [6]

$$v(r_{ij}) = \frac{\epsilon}{\alpha} \left(1 - \frac{r_{ij}}{\sigma_{ij}}\right)^\alpha H(\sigma_{ij} - r_{ij}) \quad (1)$$

where r_{ij} is the distance between particles i and j , $\sigma_{ij} = (\sigma_i + \sigma_j)/2$ is the sum of radii of two particles, and $H(x)$ is the Heaviside step function. Two models of jammed particles are considered, harmonic spheres ($\alpha = 2$) and Hertzian spheres ($\alpha = 5/2$). For both models, we use 50:50 binary mixtures of particles whose diameters are σ and 1.4σ with identical mass m . The number of particles in the system is denoted as N . Masses, lengths, and energies are measured in units of m , σ , and ϵ , respectively. The number density is expressed as $\rho = N/L^d$, where $d = 3$ is the spatial dimension.

B. Numerical generation of jammed packings

We start the preparation of packings by minimising the energy of random configurations at a sufficiently high packing fraction $\varphi_{\text{init}} = 1.0$ with the FIRE algorithm [52]. The algorithm is terminated when the condition $\max_i F_i < 10^{-12}$ is reached. Then, we perform the global compression/decompression to generate packings at a given target pressure p [53]. For harmonic spheres, pressures range over $p = 10^{-2}, 10^{-3}, \dots, 10^{-6}$ for all system sizes. For Hertzian spheres, the highest pressure is $p = 10^{-2}$ for all system sizes, and the lowest pressure is $p = 10^{-8}$ for $N = 2000$. For the case of $N = 32000$, the lowest pressure is $p = 10^{-7}$. A packing ensemble prepared with the compression/decompression-only protocols may contain samples that have finite pressure but are unstable to shear [54]. We discard such samples with a negative shear modulus when constructing the ensembles. The sizes of ensembles used in this study are given in Appendix A. After packings are generated, we recursively remove rattler particles whose number of contacts N_c satisfies $N_c \leq d$ [55].

C. Calculation of stressed and unstressed shear moduli

Here, we recap the linear response formulation of shear moduli used in this study [56–58]. Because the system is isotropic, we measure the elastic response exclusively for a shear strain in the x direction with a strain gradient in the y direction.

The elastic modulus is decomposed into two components, the affine and non-affine modulus: $G = G_A - G_N$ [59, 60]. The affine modulus (Born–Huang term) is the second derivative of total potential energy E , defined as

$$E = \sum_{\langle ij \rangle} v(r_{ij}), \quad (2)$$

with respect to the affine strain, evaluated as [56–58, 61–63]

$$G_A = \frac{1}{V} \sum_{\langle ij \rangle} \left[\left(k_{ij} + \frac{f_{ij}}{r_{ij}} \right) \frac{x_{ij}^2 y_{ij}^2}{r_{ij}^2} - f_{ij} \frac{r_{ij}}{d} \right], \quad (3)$$

where V is the volume of the simulation box, $f_{ij} = -v'(r_{ij})$ and $k_{ij} = v''(r_{ij})$ are the first and second derivatives of the potential $v(r_{ij})$ with respect to r_{ij} . The distance r_{ij} is given by the norm of the displacement vector $\mathbf{r}_{ij} = (x_{ij}, y_{ij}, z_{ij})$. The sum is taken for all bonds $\langle ij \rangle$ in the system. We note that the second term in the summation of Eq. (3) is a correction term for the finite pressure [64, 65].

The second term G_N is due to non-affine relaxation. This term is evaluated with the Hessian matrix [56–58]

$$G_N = \frac{1}{V} \Xi \cdot \mathcal{H}^{-1} \cdot \Xi, \quad (4)$$

where the i -th block of the affine force Ξ ($3N$ -dimensional vector) is provided as

$$\Xi_i = \sum_{j \neq i} \left(k_{ij} + \frac{f_{ij}}{r_{ij}} \right) \frac{x_{ij} y_{ij}}{r_{ij}} \frac{\mathbf{r}_{ij}}{r_{ij}}, \quad (5)$$

and the Hessian matrix (size $3N \times 3N$) is defined as

$$\mathcal{H} = \left[\frac{\partial^2 E}{\partial \mathbf{r}_i \partial \mathbf{r}_j} \right]_{i,j=1,2,\dots,N}, \quad (6)$$

where $\mathbf{r}_i = (x_i, y_i, z_i)$ is the coordinate of particle i . In amorphous solids, affine deformation causes an additional non-affine displacement field $\delta \mathbf{u} = \mathcal{H}^{-1} \cdot \Xi$ [56–59, 66]. This displacement field $\delta \mathbf{u}$ ($3N$ -dimensional vector) is usually obtained through the decomposition of Ξ with the normal modes of \mathcal{H} [56–58]. However, this method is computationally hard when the size of matrix \mathcal{H} becomes large. Therefore, we obtain the non-affine displacements $\delta \mathbf{u}$ via the FIRE minimisation of a cost function

$$L = \frac{1}{2} \delta \mathbf{u} \cdot \mathcal{H} \cdot \delta \mathbf{u} + \delta \mathbf{u} \cdot \Xi \quad (7)$$

instead of performing the direct diagonalization of the Hessian matrix [67]. In this minimisation, the termination condition is set to $\max_i |-\partial L / \partial \delta \mathbf{u}_i| < 10^{-8}$. This iterative method yields displacements that are identical to the direct solution of the linear equation $\mathcal{H} \cdot \delta \mathbf{u} = \Xi$ within numerical tolerance.

In the harmonic limit, the energy change ΔE caused by relative displacements $\{\mathbf{u}_i\}$ from the mechanically equilibrated position $\{\mathbf{r}_i\}$ takes the form [3, 4, 9, 61, 68]

$$\Delta E = \frac{1}{2} \sum_{\langle ij \rangle} \left(k_{ij} u_{ij,\parallel}^2 - \frac{f_{ij}}{r_{ij}} u_{ij,\perp}^2 \right), \quad (8)$$

where $u_{ij,\parallel}$ and $u_{ij,\perp}$ denote the components of the displacement parallel and perpendicular to \mathbf{r}_{ij} , respectively. This may be written compactly using the Hessian matrix: $\Delta E = \mathbf{u} \cdot \mathcal{H} \cdot \mathbf{u}$. Because the contact force $f_{ij} = -v'(r_{ij})$ is always repulsive in the jammed packings, the original state is called the stressed system. On the other hand, we have also studied the shear modulus of the unstressed system [4], where we remove f_{ij} in the Hessian matrix while maintaining k_{ij} . This case corresponds to the system where we replace the interactions between particles with relaxed (unstretched) springs of each stiffness k_{ij} . In practice, we omit the first derivatives in the Hessian matrix in the cost function (7) when calculating the shear modulus of the unstressed system. We denote the shear modulus of the stressed system by G_1 and that of the unstressed system by G_0 .

III. BEHAVIOUR OF AVERAGE SHEAR MODULUS

First, we present the critical behaviour of the ensemble-averaged shear modulus. As reported in numerous studies [6, 9, 69, 70], the shear modulus exhibits

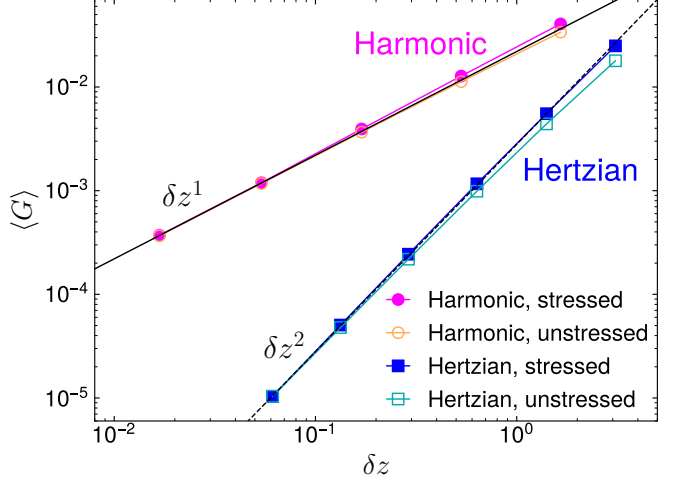


FIG. 1. Critical scaling of the average shear moduli $\langle G_1 \rangle$ and $\langle G_0 \rangle / 2$ for harmonic and Hertzian packings with $N = 32000$. The solid and dashed lines represent $\langle G \rangle \sim \delta z$ and $\langle G \rangle \sim \delta z^2$, respectively.

the following critical scaling with pressure p :

$$G \sim p^{(\alpha-3/2)/(\alpha-1)}. \quad (9)$$

In addition, the excess contact number $\delta z = z - z_{\text{iso}}$, which quantifies the distance from the isostatic point at the onset of jamming [4, 6], is known to scale as [6]:

$$\delta z \sim p^{1/(2\alpha-2)}. \quad (10)$$

Here, $z_{\text{iso}} = 2d(1 - 1/N)$ is the isostatic contact number that satisfies the Maxwell criterion, and the $1/N$ correction arises from the global zero-frequency translational modes of the finite-size systems [20]. Combining the two scaling relations yields $G \sim \delta z$ for harmonic spheres ($\alpha = 2$), and $G \sim \delta z^2$ for Hertzian spheres ($\alpha = 5/2$). As clearly shown in Fig. 1, our numerical data are consistent with these predictions: harmonic spheres exhibit the scaling $\langle G_1 \rangle \sim \delta z$, while Hertzian spheres obey $\langle G_1 \rangle \sim \delta z^2$, where $\langle \cdot \rangle$ denotes the ensemble average.

We now turn to the unstressed modulus G_0 . Similar to the stressed modulus G_1 , the unstressed modulus G_0 follows the same scaling laws for harmonic and Hertzian spheres, as shown in Fig. 1. In addition, according to the EMT for spring networks, the stressed shear modulus G_1 is expected to be twice the unstressed modulus G_0 near the jamming point [49]. To test this prediction, we plot $\langle G_0 \rangle / 2$ for both types of packings in Fig. 1. Near the jamming transition, $\langle G_0 \rangle / 2$ collapses onto $\langle G_1 \rangle$, indicating good quantitative agreement with EMT. However, further from the transition, $\langle G_1 \rangle$ exceeds $\langle G_0 \rangle / 2$, suggesting that the pre-stress e at higher pressure deviates from its critical value e_c [49]. Overall, Fig. 1 clearly demonstrates that both $\langle G_0 \rangle$ and $\langle G_1 \rangle$ obey the same scaling law within each model, while the scaling exponent itself depends on the interaction potential.

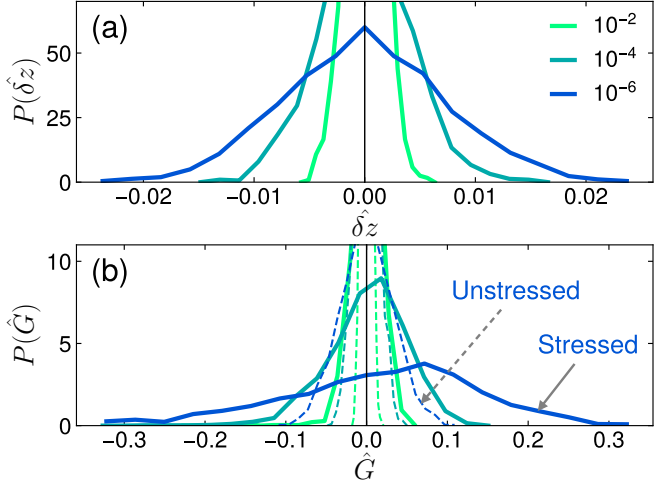


FIG. 2. Probability distributions of (a) the excess contact number δz and (b) the shear modulus G for the ensemble of Hertzian packings ($N = 32\,000$) at various pressures. To enable comparison between different pressures, each quantity X is rescaled as $\hat{X} = X/\langle X \rangle - 1$. In panel (b), the distributions of the stressed modulus G_1 are shown as solid curves, whereas those of the unstressed modulus G_0 appear as dashed curves.

IV. DIVERGENCE OF CRITICAL FLUCTUATIONS

In this section, we examine the sample-to-sample probability distributions within the ensemble used to compute the average quantities discussed above. The discussion is divided into two subsections, focusing respectively on the contact number and the shear modulus. In each case, we analyse the probability distribution of the observable of interest and quantify its fluctuations.

A. Excess contact number

We begin by presenting the sample-to-sample probability distribution of the excess contact number δz . Figure 2 (a) shows the distribution $P(\delta z)$ computed from the ensemble of Hertzian packings with $N = 32\,000$. To facilitate comparison across different pressures, we rescale the variable as $\hat{\delta}z = \delta z/\langle \delta z \rangle - 1$. As illustrated in Fig. 2 (a), the distribution is symmetric and approximately Gaussian in shape. As the pressure decreases and the system approaches the jamming transition, the distribution broadens.

We next quantify the pressure dependence of these fluctuations across the ensemble. To do so, we adopt a disorder quantifier for a generic observable X , defined as [28]

$$\chi_X = \frac{\sqrt{N \langle (X - \langle X \rangle)^2 \rangle}}{\langle X \rangle} = \frac{\sqrt{N} \sigma_X}{\langle X \rangle}, \quad (11)$$

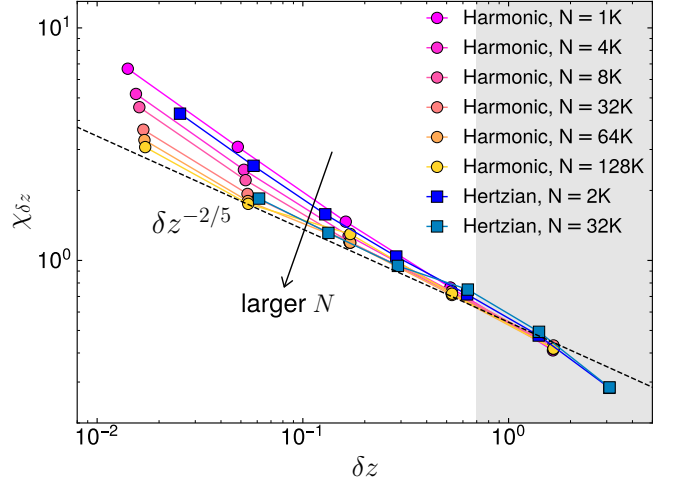


FIG. 3. Critical fluctuations of the excess contact number δz . The dashed line represents the scaling $\chi_{\delta z} \sim \delta z^{-2/5}$. The shaded region marks the glassy regime, $\delta z \gtrsim 7 \times 10^{-1}$, where this scaling behaviour is no longer expected to hold [28].

where σ_X is the standard deviation. We use this measure to characterise the fluctuations in the excess contact number ($X = \delta z$).

Figure 3 displays $\chi_{\delta z}$ for both interaction types across various system sizes. Harmonic spheres exhibit scaling behaviour $\chi_{\delta z} \sim \delta z^{-2/5}$, consistent with the findings of Giannini and coworkers [28], albeit subject to finite-size effects. On the other hand, contact-number fluctuations $\chi_{\delta z}$ of the Hertzian spheres follow a similar scaling behaviour with δz . Giannini and coworkers identified distinct regimes within the jammed phase based on the behaviour of $\chi_{\delta z}$. They reported that $\chi_{\delta z}$ becomes independent of system size at high pressures, where the scaling becomes steeper, with a more negative exponent. According to their analysis, this crossover occurs at $\delta z \approx 7 \times 10^{-1}$, and they referred to the corresponding high- δz region as the glassy regime ($\delta z \gtrsim 7 \times 10^{-1}$). Our results for both harmonic and Hertzian spheres are consistent with these observations, although we do not explore this aspect in further detail here.

B. Shear modulus

We now turn to the sample-to-sample fluctuations of the shear modulus. Figure 2 (b) displays the probability distributions of the shear moduli computed from the ensemble of Hertzian packings. Both the stressed modulus G_1 and the unstressed modulus G_0 are shown, represented by solid and dashed curves, respectively.

Compared with the excess contact number δz (Fig. 2 (a)), both moduli exhibit broader distributions at the same system size. As the pressure is lowered and the system approaches the jamming transition, these distributions become broader, mirroring the trend observed

in $P(\delta z)$. The distinction between G_1 and G_0 is also evident in Fig. 2 (b). At a given pressure, G_0 displays a narrower distribution than G_1 . Although both distributions broaden as pressure decreases, G_0 consistently remains narrower than G_1 , yet both are wider than the distribution of δz .

The shapes of the distributions also differ notably. At high pressure ($p = 10^{-2}$), both G_0 and G_1 exhibit symmetric distributions. However, at lower pressures (e.g., $p = 10^{-4}$), the peak of $P(\hat{G}_1)$ shifts towards positive values ($\hat{G}_1 > 0$), and the distribution becomes skewed. This asymmetry becomes more pronounced as the system approaches the jamming point ($p = 10^{-6}$). By contrast, $P(\hat{G}_0)$ retains a symmetric, Gaussian-like shape throughout this pressure range.

Such non-Gaussian behaviour in the distribution of G_1 has been previously reported [50], and the skewness is attributed to spatially localised vibrational modes at low frequencies, which are suppressed in the unstressed system [11]. Moreover, outliers are found only in the distribution of the stressed modulus. To quantify this, we examine the minimum and maximum values of \hat{G}_0 and \hat{G}_1 within the ensemble. While these rare samples are not visible in Fig. 2 (b) due to limited statistics, we observe that $|\min \hat{G}_1| / \max \hat{G}_1 \approx 2.5$ to 4, indicating the presence of samples with anomalously small G_1 . Consequently, a Shapiro–Wilk test applied to the raw data returns p -values close to zero, confirming strong deviation from normality. In contrast, for the unstressed modulus G_0 , we find $|\min \hat{G}_0| / \max \hat{G}_0 \approx 1$, indicating an absence of outliers. The Shapiro–Wilk test on G_0 returns p -values of approximately 0.8 or larger, even without removing any outlier data, suggesting consistency with a Gaussian distribution.

We now quantify the sample-to-sample fluctuations in the shear moduli. As noted above, the distribution of G_1 is markedly different from Gaussian and includes significant outliers, making the standard definition of the fluctuation χ_G problematic. To address this, a more robust, median-based measure has been proposed [71]:

$$\chi_{X,\text{med}} = \frac{\sqrt{N \text{ median} [(X - \langle X \rangle)^2]}}{\langle X \rangle} \quad (12)$$

which avoids the need for explicit outlier-exclusion protocols while remaining statistically meaningful. We adopt this definition for both stressed and unstressed moduli ($X = G_0, G_1$).

Figure 4 shows the fluctuation of the shear modulus as a function of δz for both moduli. For the unstressed modulus G_0 , the fluctuations exhibit a clear scaling relation: $\chi_G \sim \delta z^{-1/2}$. Finite-size effects appear negligible in this case, consistent with the narrower distribution of G_0 compared to G_1 (Fig. 2 (b)). For the stressed modulus G_1 , the fluctuations approach the same scaling $\chi_G \sim \delta z^{-1/2}$ as the system size increases. At higher pressures (i.e., larger δz), the scaling breaks down, con-

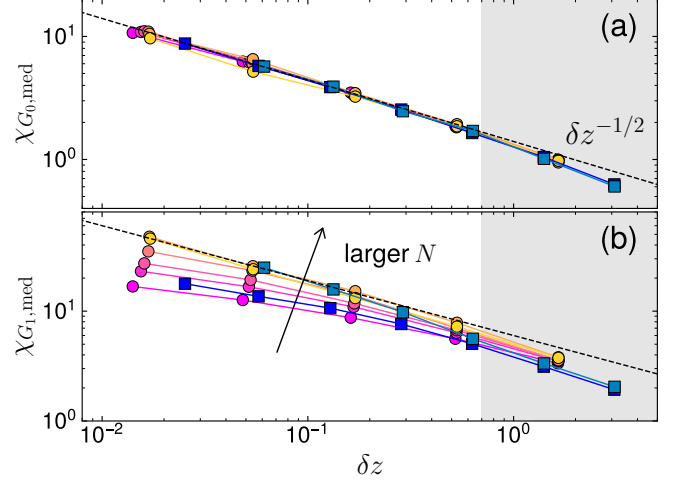


FIG. 4. Critical fluctuations of the shear moduli. The unstressed modulus G_0 and stressed modulus G_1 are shown in panels (a) and (b), respectively. The dashed lines indicate the scaling $\chi_G \sim \delta z^{-1/2}$. The legend is identical to that in Fig. 3. The shaded region denotes the glassy regime [28].

sistent with the identification of the glassy regime at $\delta z \gtrsim 7 \times 10^{-1}$ by Giannini and coworkers [28]. An important conclusion from Fig. 4 is that, in contrast with the average shear modulus (Fig. 1), the fluctuation χ_G appears independent of the interaction potential exponent α . For harmonic spheres, the scaling exponent is in agreement with previous findings [21, 28].

V. RESULTS ON TWO-DIMENSIONAL PACKINGS

Finally, we perform a similar analysis on two-dimensional packings. We use ensembles of binary disks interacting via harmonic and Hertzian potentials described in Sec. II [6]. As in three dimensions, the ensemble sizes used for this calculation are listed in Appendix A. Figure 5 shows the jamming scaling of fluctuations of the excess contact number (panel (a)), the unstressed shear modulus (panel (b)), and the stressed shear modulus (panel (c)). Analysis of the excess contact number δz reveals that the contact-number fluctuation $\chi_{\delta z}$ in two dimensions follows a different critical exponent than in three dimensions: $\chi_{\delta z} \sim \delta z^{-3/5}$ (Fig. 5 (a)), based on our numerical data. The dimensional difference in contact-number fluctuations was also reported in the literature [26] using a slightly different metric. By contrast, our analysis of shear moduli demonstrates the shear-moduli fluctuations in two dimensions diverge in the same manner as in three-dimensional systems, $\chi_G \sim \delta z^{-1/2}$ (Fig. 5 (b), (c)). This observation is consistent with previous results for harmonic packings [21], which suggested $\sigma_{G_1}/\langle G_1 \rangle \sim (pN^2)^{-1/4} \sim \delta z^{-1/2}$ in both two and three dimensions. Our results therefore

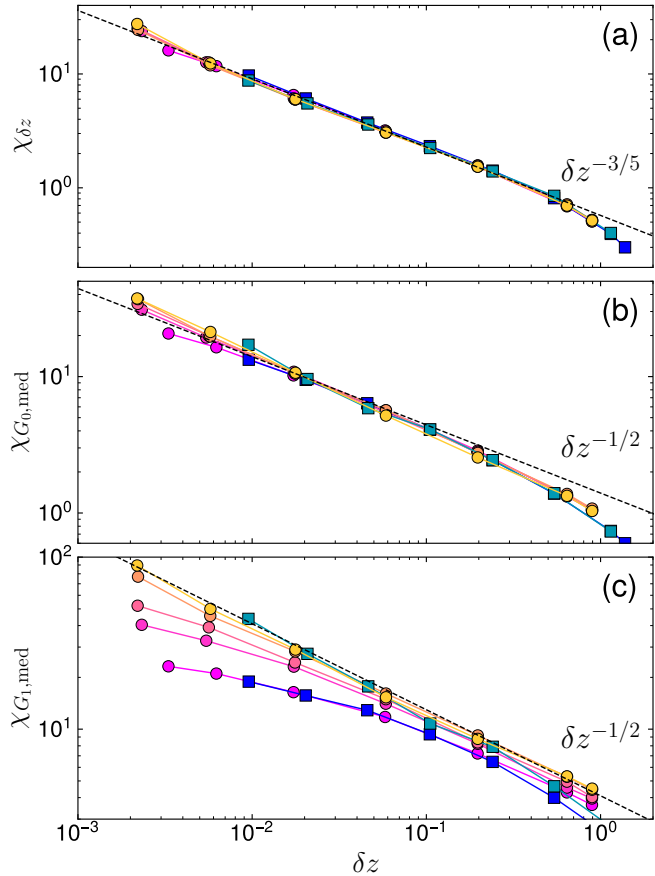


FIG. 5. Critical fluctuations in two-dimensional disk packings of harmonic and Hertzian interactions. Panels (a), (b), and (c) display data of the excess contact number, the unstressed modulus, and the stressed modulus, respectively. In panel (a), the dashed line in black represents $\chi_{\delta z} \sim \delta z^{-3/5}$. Dashed lines in panels (b) and (c) represent $\chi_G \sim \delta z^{-1/2}$. The legend is same with the case of three dimensions.

indicate that shear-modulus fluctuations are dimensionally independent, whereas contact-number fluctuations are not. Notably, the robustness with respect to the interaction potential holds for fluctuations of both quantities.

VI. CONCLUSION AND DISCUSSIONS

In this paper, we have investigated the sample-to-sample fluctuations of the shear modulus and contact number in two models of jammed packings. We have found that, while the average values exhibit critical exponents that depend on the interaction potential, the critical exponents of fluctuations display potential-independent values with respect to δz . Specifically, the fluctuation indicators scale as $\chi_{\delta z} \sim \delta z^{-2/5}$ for the excess contact number and $\chi_G \sim \delta z^{-1/2}$ for the shear modulus in three dimensions. The exponent of the shear modulus is identical for both stressed and unstressed sys-

tems. While the exponent of excess contact number is dimension-dependent, the exponent of shear moduli is identical for two- and three-dimensional packings.

As stated in the Introduction, the divergence of fluctuations implies the divergence of associated correlation lengths. Our results indicate that the exponent governing the length scale associated with contact-number fluctuations depends on spatial dimension, whereas the length scale associated with elastic-modulus fluctuations exhibits the same scaling behaviour in both two and three dimensions. The exponent controlling the divergence of elastic-modulus fluctuations coincides with that of the correlation length $l_c \sim \delta z^{-1/2}$, which characterises low-frequency vibrational modes and diverges at the jamming transition [10]. Crucially, the shear modulus of jammed packing is significantly influenced by non-affine responses to the deformation, which are known to be spatially organised over l_c under global shear [72]. Just as the four-point susceptibility reflects the growth of domain size of dynamic heterogeneity in glass-forming liquids, the divergence of χ_G manifests the increasing correlation length of the non-affine displacement fields. As the system approaches the jamming transition, these displacements become increasingly correlated over larger distances, leading to greater variability in the shear modulus between different samples. This length scale l_c related to elastic-modulus fluctuations also manifests itself in vibrational modes [10, 23, 73] and responses to local perturbation [22], and these behaviours can also be captured within EMT [49, 74]. The fact that $\chi_G \sim \delta z^{-1/2} \sim l_c$ holds across different interaction potentials and spatial dimensions strongly suggests that the elastic criticality is robustly controlled by this mesoscopic length scale, regardless of local microscopic details. By contrast, the physical implication of the length scale associated with contact-number fluctuations remains unclear. However, our results highlight the fact that those fluctuations obey different scaling exponents in two and three dimensions, while the average contact number follows a single exponent. This suggests that the spatial correlation of the contact network or geometric constraints may involve different characteristic features in dimensions.

Finally, we situate our results on elastic fluctuations in the context of the HET, which provides a theoretical framework for describing sound attenuation in amorphous solids. According to HET, the attenuation coefficient Γ and the propagation frequency Ω are related through the Rayleigh scaling [35]

$$\frac{\Gamma(\Omega)}{\omega_0} \propto \gamma \left(\frac{\Omega}{\omega_0} \right)^{d+1}, \quad (13)$$

where the disorder parameter γ is determined by spatial fluctuations of the local elastic modulus. Here, ω_0 denotes the characteristic frequency associated with the elastic correlation length [75, 76]. Several specific forms of ω_0 have been proposed, some taking it as the boson peak frequency ω_{BP} [51], or evaluating it as $\omega_G = c_T/a_0$ [50], where c_T is the sound speed of transverse

wave $c_T = \sqrt{G/(m\rho)}$ and $a_0 = \rho^{-1/d}$ is the characteristic interparticle spacing. It should be noted that HET does not provide a fully quantitative prediction of the absolute magnitude of Γ , and a system-dependent rescaling factor is generally required to achieve quantitative agreement with numerical data [50, 77].

Detailed numerical simulations have elucidated the jamming scaling laws governing sound attenuation [14]. In the low-frequency regime of the Rayleigh scattering, it follows

$$\frac{\Gamma(\Omega)}{\omega^*} \propto B \left(\frac{\Omega}{\omega^*} \right)^{d+1} \quad (14)$$

for both two and three dimensions ($d = 2, 3$), where B represents a constant of the attenuation strength. Here, ω^* denotes the onset frequency of the plateau in the vibrational density of states, and it follows the same jamming scaling law as ω_{BP} : $\omega^* \sim \omega_{\text{BP}} \sim \delta z$ [10, 11]. Consequently, if one adopts the HET prediction with $\omega_0 = \omega_{\text{BP}}$, the predicted prefactor γ becomes a constant $\gamma \sim \delta z^0$ in two and three dimensions. By contrast, if one instead chooses $\omega_0 = \omega_G$, whose jamming scaling is $\omega_G \sim \delta z^{1/2}$, the corresponding prefactor γ becomes dimension-dependent: $\gamma \sim \delta z^{-1}$ in two dimensions and $\gamma \sim \delta z^{-3/2}$ in three dimensions.

Recent simulations of soft-core and Lennard-Jones systems have demonstrated that this disorder parameter could be estimated from sample-to-sample fluctuations [50, 51, 78] by assuming the spatial correlations of local elastic moduli are short-ranged and saturate upon coarse-graining [40, 41, 61, 79]. This approach also has the merit of sidestepping the direct evaluation of local elastic moduli [41, 47], and it is claimed that *spatial* fluctuations of shear modulus γ can be replaced by the *sample-to-sample* fluctuations χ_G^2 [50, 51]. Our present result of jammed packings shows that $\chi_G^2 \sim \delta z^{-1}$ regardless of the spatial dimension, and this is indeed aligned with numerical simulations of acoustic attenuation in two-dimensional packings [14] if we select ω_G as ω_0 in Eq. (13) (note that the jamming scaling of the disorder parameter γ varies on the selection of the normalisation frequency ω_0).

Overall, our findings highlight that jamming scaling laws play a central role in governing elastic fluctuations and their impact on the acoustic attenuation. Nonetheless, the numerical character of the disorder parameter employed in HET remains poorly characterised; clarifying which fluctuations it captures and their scaling near jamming is necessary before HET can be applied to the attenuation prefactor. To resolve these issues, systematic studies at lower pressures and larger system sizes, direct measurements of spatial correlations of local elastic moduli, and quantitative comparisons with acoustic scattering data will be crucial [77, 80–84]. Pursuing these directions should clarify how universal the observed scalings are and under which physical conditions the HET-based description becomes predictive.

Appendix A: Enumeration of the number of packings

In this appendix, we present the sizes of packing ensembles that are used in the present study. Table I shows the numbers of three-dimensional packings, whereas Table II shows the numbers of two-dimensional packings. All cases of the number of particles N , pressures p , and interaction potentials are presented in the two tables.

CONFLICTS OF INTEREST

There are no conflicts to declare.

DATA AVAILABILITY

Data relevant to this work can be accessed at the University of Osaka Institutional Knowledge Archive [85].

ACKNOWLEDGMENTS

KS acknowledges Yusuke Hara for useful discussions in the early stages of this work. This work is supported by JSPS KAKENHI Grant Number 25H01519 and JST ERATO Grant Number JPMJER2401.

[1] A. J. Liu and S. R. Nagel, The Jamming Transition and the Marginally Jammed Solid, *Annual Review of Condensed Matter Physics* **1**, 347 (2010).

[2] M. van Hecke, Jamming of soft particles: geometry, mechanics, scaling and isostaticity, *Journal of Physics: Condensed Matter* **22**, 033101 (2010).

[3] M. Wyart, S. R. Nagel, and T. A. Witten, Geometric origin of excess low-frequency vibrational modes in weakly connected amorphous solids, *Europhysics Letters* **72**, 486 (2005).

[4] M. Wyart, L. E. Silbert, S. R. Nagel, and T. A. Witten, Effects of compression on the vibrational modes of marginally jammed solids, *Physical Review E* **72**, 051306 (2005).

[5] C. S. O’Hern, S. A. Langer, A. J. Liu, and S. R. Nagel, Random Packings of Frictionless Particles, *Physical Review Letters* **88**, 075507 (2002).

[6] C. S. O’Hern, L. E. Silbert, A. J. Liu, and S. R. Nagel, Jamming at zero temperature and zero applied stress: The epitome of disorder, *Physical Review E* **68**, 011306 (2003).

[7] T. G. Mason, J. Bibette, and D. A. Weitz, Elasticity of Compressed Emulsions, *Physical Review Letters* **75**, 2051 (1995).

TABLE I. The number of samples of three-dimensional packings. The numbers are presented for each number of particles N and each pressure p .

N / p	10^{-2}	10^{-3}	10^{-4}	10^{-5}	10^{-6}	10^{-7}	10^{-8}
Harmonic							
1000	11 958	11 825	11 472	10 693	10 691	-	-
4000	10 192	10 157	10 054	9832	9820	-	-
8000	5800	5796	5751	5700	5700	-	-
32 000	1530	1530	1527	1513	1510	-	-
64 000	690	690	688	681	681	-	-
128 000	407	407	407	407	405	-	-
Hertzian							
2000	8047	8044	8014	7943	7987	7960	7935
32 000	1800	1800	1799	1794	1767	1742	-

TABLE II. The number of samples of two-dimensional packings. The numbers are presented for each number of particles N and each pressure p .

N / p	2×10^{-2}	10^{-2}	10^{-3}	10^{-4}	10^{-5}	10^{-6}	10^{-7}	10^{-8}
Harmonic								
1000	10 945	10 556	10 312	9628	9145	9075	9126	-
4000	6013	6017	5981	5863	5510	4718	4551	-
8000	3709	3708	3704	3664	3724	3538	3421	-
32 000	1330	1330	1330	1329	1317	1298	1163	-
64 000	696	696	696	695	694	648	426	-
Hertzian								
1000	7992	7986	7946	7820	7589	7135	6964	5699
32 000	-	576	576	576	574	575	556	289

[8] T. S. Majmudar, M. Sperl, S. Luding, and R. P. Behringer, Jamming Transition in Granular Systems, *Physical Review Letters* **98**, 058001 (2007).

[9] W. G. Ellenbroek, E. Somfai, M. van Hecke, and W. van Saarloos, Critical Scaling in Linear Response of Frictionless Granular Packings near Jamming, *Physical Review Letters* **97**, 258001 (2006).

[10] L. E. Silbert, A. J. Liu, and S. R. Nagel, Vibrations and Diverging Length Scales Near the Unjamming Transition, *Physical Review Letters* **95**, 098301 (2005).

[11] H. Mizuno, H. Shiba, and A. Ikeda, Continuum limit of the vibrational properties of amorphous solids, *Proceedings of the National Academy of Sciences* **114**, E9767 (2017).

[12] N. Xu, V. Vitelli, M. Wyart, A. J. Liu, and S. R. Nagel, Energy Transport in Jammed Sphere Packings, *Physical Review Letters* **102**, 038001 (2009).

[13] V. Vitelli, N. Xu, M. Wyart, A. J. Liu, and S. R. Nagel, Heat transport in model jammed solids, *Physical Review E* **81**, 021301 (2010).

[14] H. Mizuno and A. Ikeda, Phonon transport and vibrational excitations in amorphous solids, *Physical Review E* **98**, 062612 (2018).

[15] P. Olsson and S. Teitel, Critical Scaling of Shear Viscosity at the Jamming Transition, *Physical Review Letters* **99**, 178001 (2007).

[16] H. E. Stanley, *Introduction to Phase Transitions and Critical Phenomena* (Oxford University Press, 1971).

[17] J. J. Binney, N. J. Dowrick, A. J. Fisher, and M. E. J. Newman, *The Theory of Critical Phenomena: An Introduction to the Renormalization Group* (Oxford University Press, 1992).

[18] N. Goldenfeld, *Lectures on Phase Transitions and the Renormalization Group* (CRC Press, 1992).

[19] H. Nishimori and G. Ortiz, *Elements of Phase Transitions and Critical Phenomena* (Oxford University Press, 2010).

[20] C. P. Goodrich, A. J. Liu, and S. R. Nagel, Finite-Size Scaling at the Jamming Transition, *Physical Review Letters* **109**, 095704 (2012).

[21] C. P. Goodrich, S. Dagois-Bohy, B. P. Tighe, M. van Hecke, A. J. Liu, and S. R. Nagel, Jamming in finite systems: Stability, anisotropy, fluctuations, and scaling, *Physical Review E* **90**, 022138 (2014).

[22] E. Lerner, E. DeGiuli, G. Düring, and M. Wyart, Breakdown of continuum elasticity in amorphous solids, *Soft Matter* **10**, 5085 (2014).

[23] L. Yan, E. DeGiuli, and M. Wyart, On variational arguments for vibrational modes near jamming, *Europhysics Letters* **114**, 26003 (2016).

[24] C. P. Goodrich, A. J. Liu, and J. P. Sethna, Scaling ansatz for the jamming transition, *Proceedings of the National Academy of Sciences* **113**, 9745 (2016).

[25] D. Hexner, A. J. Liu, and S. R. Nagel, Two Diverging Length Scales in the Structure of Jammed Packings, *Physical Review Letters* **121**, 115501 (2018).

[26] D. Hexner, P. Urbani, and F. Zamponi, Can a Large Packing be Assembled from Smaller Ones?, *Physical Review Letters* **123**, 068003 (2019).

[27] H. Ikeda, Control parameter dependence of fluctuations near jamming, *The Journal of Chemical Physics* **158**, 056101 (2023).

[28] J. A. Giannini, E. Lerner, F. Zamponi, and M. L. Manning, Scaling regimes and fluctuations of observables in computer glasses approaching the unjamming transition, *The Journal of Chemical Physics* **160**, 034502 (2024).

[29] V. L. Gurevich, D. A. Parshin, and H. R. Schober, Anharmonicity, vibrational instability, and the Boson peak in glasses, *Physical Review B* **67**, 094203 (2003).

[30] S. Franz, G. Parisi, P. Urbani, and F. Zamponi, Universal spectrum of normal modes in low-temperature glasses, *Proceedings of the National Academy of Sciences* **112**, 14539 (2015).

[31] T. Damart, A. Tanguy, and D. Rodney, Theory of harmonic dissipation in disordered solids, *Physical Review B* **95**, 054203 (2017).

[32] M. Baggio and A. Zacccone, Theory of sound attenuation in amorphous solids from nonaffine motions, *Journal of Physics: Condensed Matter* **34**, 215401 (2022).

[33] F. Vogel and M. Fuchs, Vibrational Phenomena in Glasses at Low Temperatures Captured by Field Theory of Disordered Harmonic Oscillators, *Physical Review Letters* **130**, 236101 (2023).

[34] F. Vogel, P. Baumgärtel, and M. Fuchs, Self-Consistent Current Response Theory of Unjamming and Vibrational Modes in Low-Temperature Amorphous Solids, *Physical Review X* **15**, 011030 (2025).

[35] W. Schirmacher and G. Ruocco, Heterogeneous Elasticity: The Tale of the Boson Peak, in *Low-Temperature Thermal and Vibrational Properties of Disordered Solids*, edited by M. A. Ramos (WORLD SCIENTIFIC (EUROPE), 2022) Chap. 9, pp. 331–373.

[36] W. Schirmacher, Thermal conductivity of glassy materials and the “boson peak”, *Europhysics Letters* **73**, 892 (2006).

[37] W. Schirmacher, G. Ruocco, and T. Scopigno, Acoustic Attenuation in Glasses and its Relation with the Boson Peak, *Physical Review Letters* **98**, 025501 (2007).

[38] A. Marruzzo, W. Schirmacher, A. Fratalocchi, and G. Ruocco, Heterogeneous shear elasticity of glasses: the origin of the boson peak, *Scientific Reports* **3**, 1407 (2013).

[39] W. Schirmacher, T. Scopigno, and G. Ruocco, Theory of vibrational anomalies in glasses, *Journal of Non-Crystalline Solids* **407**, 133 (2015).

[40] M. Tsamados, A. Tanguy, C. Goldenberg, and J.-L. Barrat, Local elasticity map and plasticity in a model Lennard-Jones glass, *Physical Review E* **80**, 026112 (2009).

[41] H. Mizuno, S. Mossa, and J.-L. Barrat, Measuring spatial distribution of the local elastic modulus in glasses, *Physical Review E* **87**, 042306 (2013).

[42] H. Mizuno, L. E. Silbert, and M. Sperl, Spatial Distributions of Local Elastic Moduli Near the Jamming Transition, *Physical Review Letters* **116**, 068302 (2016).

[43] G. Baldi, V. M. Giordano, G. Monaco, and B. Ruta, Sound Attenuation at Terahertz Frequencies and the Boson Peak of Vitreous Silica, *Physical Review Letters* **104**, 195501 (2010).

[44] G. Baldi, V. M. Giordano, B. Ruta, R. Dal Maschio, A. Fontana, and G. Monaco, Anharmonic Damping of Terahertz Acoustic Waves in a Network Glass and Its Effect on the Density of Vibrational States, *Physical Review Letters* **112**, 125502 (2014).

[45] H. Mizuno, S. Mossa, and J.-L. Barrat, Relation of vibrational excitations and thermal conductivity to elastic heterogeneities in disordered solids, *Physical Review B* **94**, 144303 (2016).

[46] K. Shiraishi, H. Mizuno, and A. Ikeda, Non-phononic density of states of two-dimensional glasses revealed by random pinning, *The Journal of Chemical Physics* **158**, 174502 (2023).

[47] H. Mizuno, S. Mossa, and J.-L. Barrat, Acoustic excitations and elastic heterogeneities in disordered solids, *Proceedings of the National Academy of Sciences* **111**, 11949 (2014).

[48] L. Wang, L. Berthier, E. Flenner, P. Guan, and G. Szaamel, Sound attenuation in stable glasses, *Soft Matter* **15**, 7018 (2019).

[49] E. DeGiuli, A. Laversanne-Finot, G. Düring, E. Lerner, and M. Wyart, Effects of coordination and pressure on sound attenuation, boson peak and elasticity in amorphous solids, *Soft Matter* **10**, 5628 (2014).

[50] G. Kapteijns, D. Richard, E. Bouchbinder, and E. Lerner, Elastic moduli fluctuations predict wave attenuation rates in glasses, *The Journal of Chemical Physics* **154**, 081101 (2021).

[51] S. Mahajan and M. Pica Ciamarra, Unifying Description of the Vibrational Anomalies of Amorphous Materials, *Physical Review Letters* **127**, 215504 (2021).

[52] J. Guénolé, W. G. Nöhring, A. Vaid, F. Houllé, Z. Xie, A. Prakash, and E. Bitzek, Assessment and optimization of the fast inertial relaxation engine (FIRE) for energy minimization in atomistic simulations and its implementation in LAMMPS, *Computational Materials Science* **175**, 109584 (2020).

[53] C. P. Goodrich, *Unearthing the Anticrystal: Criticality in the Linear Response of Disordered Solids*, Ph.D. thesis, University of Pennsylvania (2015).

[54] S. Dagois-Bohy, B. P. Tighe, J. Simon, S. Henkes, and M. van Hecke, Soft-Sphere Packings at Finite Pressure but Unstable to Shear, *Physical Review Letters* **109**, 095703 (2012).

[55] P. Charbonneau, E. I. Corwin, G. Parisi, and F. Zamponi, Jamming Criticality Revealed by Removing Localized Buckling Excitations, *Physical Review Letters* **114**, 125504 (2015).

[56] C. Maloney and A. Lemaître, Universal Breakdown of Elasticity at the Onset of Material Failure, *Physical Review Letters* **93**, 195501 (2004).

[57] C. E. Maloney and A. Lemaître, Amorphous systems in athermal, quasistatic shear, *Physical Review E* **74**, 016118 (2006).

[58] A. Lemaître and C. Maloney, Sum Rules for the Quasi-Static and Visco-Elastic Response of Disordered Solids at Zero Temperature, *Journal of Statistical Physics* **123**, 415 (2006).

[59] S. Alexander, Amorphous solids: their structure, lattice dynamics and elasticity, *Physics Reports* **296**, 65 (1998).

[60] N. W. Ashcroft and N. D. Mermin, *Solid State Physics* (Saunders College, 1976).

[61] H. Mizuno, K. Saitoh, and L. E. Silbert, Elastic moduli and vibrational modes in jammed particulate packings, *Physical Review E* **93**, 062905 (2016).

[62] J. F. Lutsko, Generalized expressions for the calculation of elastic constants by computer simulation, *Journal of Applied Physics* **65**, 2991 (1989).

- [63] T. H. K. Barron and M. L. Klein, Second-order elastic constants of a solid under stress, *Proceedings of the Physical Society* **85**, 523 (1965).
- [64] J. P. Wittmer, H. Xu, P. Polińska, C. Gillig, J. Helfferich, F. Weysser, and J. Baschnagel, Compressibility and pressure correlations in isotropic solids and fluids, *The European Physical Journal E* **36**, 131 (2013).
- [65] J. P. Wittmer, H. Xu, P. Polińska, F. Weysser, and J. Baschnagel, Shear modulus of simulated glass-forming model systems: Effects of boundary condition, temperature, and sampling time, *The Journal of Chemical Physics* **138**, 12A533 (2013).
- [66] A. Zaccone and E. Scossa-Romano, Approximate analytical description of the nonaffine response of amorphous solids, *Physical Review B* **83**, 184205 (2011).
- [67] Y. Hara, H. Mizuno, and A. Ikeda, Microrheology near jamming, *Soft Matter* **19**, 6046 (2023).
- [68] W. G. Ellenbroek, M. van Hecke, and W. van Saarloos, Jammed frictionless disks: Connecting local and global response, *Physical Review E* **80**, 061307 (2009).
- [69] H. A. Makse, N. Gland, D. L. Johnson, and L. M. Schwartz, Why Effective Medium Theory Fails in Granular Materials, *Physical Review Letters* **83**, 5070 (1999).
- [70] P. Wang, S. Zhang, P. Tuckman, N. T. Ouellette, M. D. Shattuck, and C. S. O'Hern, Shear response of granular packings compressed above jamming onset, *Physical Review E* **103**, 022902 (2021).
- [71] G. Kapteijns, E. Bouchbinder, and E. Lerner, Unified quantifier of mechanical disorder in solids, *Physical Review E* **104**, 035001 (2021).
- [72] G. Düring, E. Lerner, and M. Wyart, Phonon gap and localization lengths in floppy materials, *Soft Matter* **9**, 146 (2013).
- [73] M. Shimada, H. Mizuno, M. Wyart, and A. Ikeda, Spatial structure of quasilocalized vibrations in nearly jammed amorphous solids, *Physical Review E* **98**, 060901 (2018).
- [74] M. Wyart, Scaling of phononic transport with connectivity in amorphous solids, *Europhysics Letters* **89**, 64001 (2010).
- [75] W. Schirmacher, C. Tomaras, B. Schmid, G. Baldi, G. Viliani, G. Ruocco, and T. Scopigno, Sound attenuation and anharmonic damping in solids with correlated disorder, *Condensed Matter Physics* **13**, 23606 (2010).
- [76] W. Schirmacher, Some comments on fluctuating-elasticity and local oscillator models for anomalous vibrational excitations in glasses, *Journal of Non-Crystalline Solids* **357**, 518 (2011).
- [77] C. Caroli and A. Lemaître, Fluctuating Elasticity Fails to Capture Anomalous Sound Scattering in Amorphous Solids, *Physical Review Letters* **123**, 055501 (2019).
- [78] G. Szamel and E. Flenner, Sound attenuation in glasses, *The Journal of Chemical Physics* **163**, 050903 (2025).
- [79] A. Shakerpoor, E. Flenner, and G. Szamel, Stability dependence of local structural heterogeneities of stable amorphous solids, *Soft Matter* **16**, 914 (2020).
- [80] C. Caroli and A. Lemaître, Key role of retardation and non-locality in sound propagation in amorphous solids as evidenced by a projection formalism, *The Journal of Chemical Physics* **153**, 144502 (2020).
- [81] G. Szamel and E. Flenner, Microscopic analysis of sound attenuation in low-temperature amorphous solids reveals quantitative importance of non-affine effects, *The Journal of Chemical Physics* **156**, 144502 (2022).
- [82] S. Mahajan and M. Pica Ciamarra, Heterogeneous attenuation of sound waves in three-dimensional amorphous solids, *Physical Review E* **109**, 024605 (2024).
- [83] E. Flenner and G. Szamel, The origin of sound damping in amorphous solids: Defects and beyond, *Science Advances* **11**, eadu6097 (2025).
- [84] E. Flenner and G. Szamel, Defects, Sound Damping, and the Boson Peak in Amorphous Solids, *The Journal of Physical Chemistry B* **129**, 1855 (2025).
- [85] K. Shiraishi and H. Mizuno, Dataset: Critical fluctuations of elastic moduli in jammed solids (2025).